Spectrum of power laws for curved hand movements

Dongsung Huh[a,b] and Terrence J. Sejnowski[a,c,1]

[a]Howard Hughes Medical Institute, The Salk Institute for Biological Studies, La Jolla, CA 92037; [b]Gatsby Computational Neuroscience Unit, University College London, London W1T 4JG, United Kingdom; and [c]Division of Biological Sciences, University of California at San Diego, La Jolla, CA 92161

Contributed by Terrence J. Sejnowski, May 28, 2015 (sent for review December 31, 2014; reviewed by Tamar Flash and Steven W. Zucker)

In a planar free-hand drawing of an ellipse, the speed of movement is proportional to the −1/3 power of the local curvature, which is widely thought to hold for general curved shapes. We investigated this phenomenon for general curved hand movements by analyzing an optimal control model that maximizes a smoothness cost and exhibits the −1/3 power for ellipses. For the analysis, we introduced a new representation for curved movements based on a moving reference frame and a dimensionless angle coordinate that revealed scale-invariant features of curved movements. The analysis confirmed the power law for drawing ellipses but also predicted a spectrum of power laws with exponents ranging between 0 and −2/3 for simple movements that can be characterized by a single angular frequency. Moreover, it predicted mixtures of power laws for more complex, multifrequency movements that were confirmed with human drawing experiments. The speed profiles of arbitrary doodling movements that exhibit broadband curvature profiles were accurately predicted as well. These findings have implications for motor planning and predict that movements only depend on one radian of angle coordinate in the past and only need to be planned one radian ahead.

optimal control | motor system | free-hand drawing | power law

Natural body movements have surprising regularities despite the complexity of the movements and the many degrees of freedom that are involved. These regularities provide insights into principles underlying the mechanisms that generate the movements. We investigate here conditions when a known regularity fails to adequately describe motor behavior, which adds new insights into how movements are generated by the nervous system.

One of the best-studied movement regularities is the inverse relationship between the speed and curvature of 2D hand movements observed when subjects are instructed to freely draw curved shapes such as ellipses, which follow a remarkably simple power law (1):

$$v(t) \propto \kappa(t)^{-\beta}, \ (\beta \approx 1/3). \qquad [1]$$

This empirical relationship is called the one-third power law between speed and curvature, or equivalently, the two-thirds power law between angular speed and curvature. On a log curvature vs. log speed plot of hand movement, the power law appears as a single straight line with a slope of $-1/3$ (Fig. 1*A*).

However, deviations from Eq. **1** have been observed for some movement trajectories. One class of deviation occurs when the curvature changes sign: The power law predicts the speed should diverge to infinity as the curvature approaches zero, which is physically implausible, whereas actual movements exhibit smooth, finite speed profiles at such inflection points. Deviations have also been observed for movements without inflection points (1–4). These noninflectional deviations occur in complex movements and are characterized by fragmentation of the log speed vs. log curvature plot into multiple line segments (Fig. 1*B*). These observations led to the segmented control hypothesis that complex movements could be generated by concatenating smaller and simpler movement segments, each of which separately obeys the one-third power law (2, 3). Unlike inflectional deviations, however, the origin and properties of noninflectional deviations, as well as the conditions that cause fragmentation, are poorly understood.

A variety of competing theoretical models have been proposed to explain the power law for curved trajectories (3–10). These models can reproduce the one-third power law relationship for simple, ellipse drawing movements, and most of them do not exhibit inflectional deviations (for an exception, see refs. 4 and 7). However, it is not known whether these models exhibit the observed fragmentation of power law for complex trajectories, because most of them have only been examined for a narrow range of movements.

Here, we investigate one of the models, the minimum-jerk model, for a wide range of convex movement paths without inflection points. Remarkably, this optimal control model is known to reproduce accurately the one-third power law for simple, ellipse drawing movements (8), as well as the apparent fragmentation observed for more complex movement trajectories without invoking the segmented control hypothesis (3, 9, 10). This suggests that there may be additional regularities underlying fragmentation, apart from the one-third power law relationship. Thus, a closer examination of the minimum-jerk model could lead to a more comprehensive understanding of the regularities in curved hand movements.

The following questions will be addressed: First, how does the power law arise from the optimality principle? Second, what determines the particular exponent β? Finally, how can complex movements be characterized, and why do they deviate from power law behaviors?

New Representation for Curved Movements

The minimum-jerk model minimizes the total squared-jerk cost over a trajectory, where jerk is the second-order time derivative of hand velocity (11). It also requires additional information about the movement, such as the duration and path shape, which are provided as constraints (3, 9).

The model is usually represented in Cartesian frame with time coordinate, in which the jerk cost is expressed as $\mathcal{L} = (d^2v_x/dt^2)^2 + (d^2v_y/dt^2)^2$. In this representation, however, the explicit path constraint makes the optimization problem difficult to solve. In previous studies, the path constraint was instead approximated

Significance

In curved hand movements around ellipses, the speed tends to scale inversely with the curvature with a power law having an exponent of −1/3. We examined whether this well-known regularity in motor planning holds for more general shapes. Using an optimality principle, we identified a set of basis shapes, each with a single characteristic angular frequency, which subjects drew with power laws whose exponents ranged from 0 to −2/3. More general movements exhibited linear mixtures of power laws. The speed of arbitrary doodling movements with a broad spectrum of frequencies could also be predicted from the curvature with high accuracy.

Author contributions: D.H. and T.J.S. designed research; D.H. performed research; and D.H. and T.J.S. wrote the paper.

Reviewers: T.F., Weizmann Institute; and S.W.Z., Yale University.

The authors declare no conflict of interest.

[1]To whom correspondence should be addressed. Email: terry@salk.edu.

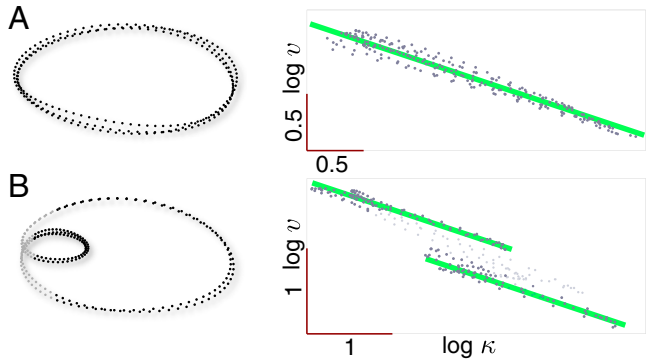

Fig. 1. Illustration of power law relationships for an ellipse and a complex movement trajectory. (*A*) An ellipse drawing movement. The data points (black dots) are samples along the hand trajectory at equal time intervals (*Left*) and form a straight line on a log speed–log curvature scale with approximate slope of −1/3 (green line; *Right*). (*B*) A more complex movement trajectory consisting of two conjuncted elliptic shapes of different sizes (*Left*). The data points plotted on a log speed–log curvature scale form two straight lines with approximate slopes of −1/3 (green lines; *Right*). The apparent fragmentation into two segments is an example of a noninflectional deviation from the simple power law.

with a number of point constraints (via points) along the path, which allowed the model to be solved with numerical optimization (3, 9, 11).

Here, we take an alternative, analytic approach to finding optimal solutions. Because the path constraint only restricts movement direction but not speed, the optimization problem can be significantly simplified if represented in a way that separates these variables. A similar approach is used in robotics for efficient trajectory planning (12). This representation requires replacing both the frame of reference and time coordinate for the path.

First, we replace the usual Cartesian frame with a moving reference frame (Frenet–Serret frame) whose basis vectors rotate with the direction of movement (Fig. 2*B*) (9, 10, 13). This frame naturally separates magnitude and directional information of a movement: (*i*) An instantaneous velocity vector is represented by its speed and tangent direction, and (*ii*) a velocity profile along the path is represented by two scalar profiles, the speed profile and the curvature profile; the latter describes how the tangent vector rotates along the path.

Although the curvature profile in principle carries the full directional information of a movement, it fails to uniquely define the path shape when represented as a function of time, $\{\kappa(t)\}$. This is because the time parameterization, and thus the path shape defined by $\{\kappa(t)\}$, depends on the speed profile. In previous approaches, this problem was resolved by replacing the time coordinate with the arc-length coordinate (9, 10, 13). Here, we instead introduce the orientation of the tangent vector as the new coordinate system, the angle coordinate, θ (Fig. 2*B*); this can be understood as the arc-length coordinate normalized by the local curvature, which is the natural length scale of the curve. The angle coordinate is dimensionless and scale-invariant—a point on a trajectory that is scaled in time or size has the same angular coordinate value—a property that has fundamental importance for our later analysis. Note that for convex paths without inflection points, θ changes monotonically along the paths, and therefore is a valid coordinate.

Minimum-Jerk Solution in the New Representation

In the angle coordinate system, a curvature profile uniquely defines the shape of a movement path up to translations, independently of the speed profile. Because the path constraint is implicitly incorporated into the representation, it only restricts the curvature profile without affecting the speed profile.

In this representation, the total squared-jerk cost becomes the following (*Appendix A*):

$$\int \mathcal{L}\, dt = \int \kappa^3 v^5 \left(\left(2\dot{z}^2 + \ddot{z} + \dot{h}z - 1 \right)^2 + \left(3\dot{z} + \dot{h} \right)^2 \right) d\theta, \qquad [2]$$

where the dot notation represents differentiation by angle, and $z = \log(v/v_o)$ $h = \log(\kappa/\kappa_o)$ are, respectively, the log speed and the log curvature with arbitrary dimensional constants v_o, κ_o. Given the log curvature profile $\{h(\theta)\}$ of the movement path, the log speed profile $\{z(\theta)\}$ can be obtained by optimizing Eq. **2** subject only to the movement duration constraint.

The optimality condition for the model, obtained analytically from the Euler–Lagrange equation, is given by the following (*Appendix B*):

$$\begin{aligned} \lambda = \kappa^4 v^6 \Big(& 5 + 2\dddot{z}\dot{z} - 30\ddot{z} - 10\ddot{h} - 25\dot{h}^2 + 82\dot{h}\dot{z}^3 + 40\dot{z}^4 \\ & + \dot{z}\left(2\dddot{h} + 14\ddot{h}\dot{h} - 90\dot{h} + 12\dot{h}^3 \right) \\ & + \dot{z}^2\left(20\ddot{h} + 55\dot{h}^2 - 75 \right) + 15\ddot{z}^2 \\ & + \ddot{z}\left(82\dot{z}^2 + 90\dot{h}\dot{z} + 8\ddot{h} + 22\dot{h}^2 \right) + \dddot{z}\left(20\dot{z} + 12\dot{h} \right) \Big), \end{aligned} \qquad [3]$$

where λ is a Lagrange multiplier that incorporates the duration constraint. This equation describes the minimum-jerk relationship between the curvature and speed profiles. In the following sections, we analyze this result to discover the hidden regularities of curved hand movements.

Spiral Movements

A rare case for which the nonlinear Euler–Lagrange equation in [**3**] can be exactly solved in closed form is a logarithmic spiral path. It has a simple log curvature profile that grows linearly with the angle, $\kappa(\theta) = \kappa_o e^{a\theta}$, and exhibits a scale-free shape. The analytic

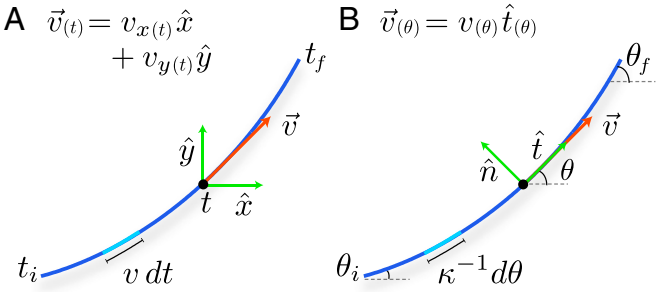

Fig. 2. Comparison between Cartesian and moving frame representations for curved hand movements. (*A*) Typically, a velocity profile is represented in a Cartesian frame, i.e., in terms of x–y components, as functions of time: $\{v_x(t)\}, \{v_y(t)\}$. $\hat{x}, \hat{y}$ are the Cartesian basis vectors. (*B*) Instead, we use a moving frame with unit tangent and normal vectors $\hat{t}, \hat{n}$ as the basis vectors (Frenet–Serret frame), and the angular direction of the tangent vector, θ, as the new coordinate along the path. In this representation, a velocity profile can be represented by the speed and the curvature profiles: $\{v(\theta)\}, \{\kappa(\theta)\}$. These two representations are interchangeable: The time coordinate can be converted to an angle coordinate, $v\, dt = d\theta/\kappa$, and the x–y components of the velocity profile are $v_x = v\cos(\theta)$, $v_y = v\sin(\theta)$. Note that θ increases by 2π with each rotation.

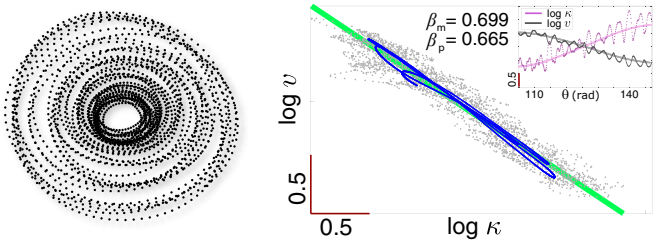

Fig. 3. Power law relationship for spiral movements. (*Left*) A spiral trajectory drawn by a subject (a circular trajectory with slowly changing radius). (*Right*) The corresponding log curvature–log speed plot. Gray dots: raw data. Blue dots: low-pass–filtered data. Green line: a straight line with −2/3 slope. Predicted $\beta_p = 0.667$ and measured $\beta_m = 0.699$. (*Inset*) The log curvature and log speed profiles vs. angle coordinate for raw (dots) and filtered data (smooth curve). (Scale bar: 0.5.)

solution for this spiral path is $v(\theta) = v_o e^{-(2/3)a\theta}$ (*Appendix C*), which is indeed a power law relationship:

$$v(\theta) \propto \kappa(\theta)^{-2/3} \quad \text{(spirals)}. \qquad [4]$$

However, this predicts an exponent of $\beta = 2/3$, not the expected one-third power law relationship in Eq. **1**. In addition to this analytical result, numerical optimization of the cost function robustly confirms the two-thirds power law relationship for other spiral path shapes, including Archimedean spirals, hyperbolic spirals, and Fermat's spirals, as well as arbitrary spirals with slowly changing curvature profiles.

To test this result, we recorded spiral drawing movements, i.e., circular movements with slowly changing radii, from $N = 8$ subjects (*Materials and Methods* and Fig. 3). The average power law exponent was $\beta = 0.697 \pm 0.052$ (mean and SD), confirming the predicted power law exponent, which is significantly different from 1/3.

This result demonstrates that curved hand movements can exhibit a power law that systematically deviates from the one-third power law. It also raises new questions: Ellipse drawing exhibits the one-third power law, so what is different about spiral drawing? Are these power laws two separate, unrelated phenomena, or is there a continuous spectrum of power laws? If so, which geometric feature of the curve is important in determining the power law exponent?

Angular Frequency: A Scale-Invariant Geometric Feature

The one-third power law for elliptic movements is invariant to the physical scale of the movements: It holds robustly across a wide range of sizes and speeds. The minimum-jerk model also generates movements that are scale-invariant because the cost function in Eq. **2** is dimensionless except for an overall constant factor $\kappa_o^3 v_o^5$; changing the overall movement size or duration should not affect the qualitative properties of minimum-jerk solutions. Therefore, the power law exponent predicted by the model can depend only on scale-free geometric features.

A salient difference between elliptic and spiral curves is the frequency with which their curvature profiles vary: The curvature of a spiral changes gradually compared with the frequent variations of the curvature along an ellipse. Here, we define "angular frequency" of a curve as the number of curvature oscillations per unit angle of θ, which we choose to be one full rotation, or 2π radians. For example, an elliptic path is characterized by angular frequency 2, because its curvature profile oscillates twice per one rotation of θ. In contrast, a logarithmic spiral is a limiting case whose characteristic angular frequency approaches zero, because its log curvature grows monotonically, i.e., with an infinite period.

Angular frequency is a scale-invariant property of path shape that does not depend on the overall movement speed or size; this property derives from the scale-invariant nature of the angle coordinate. In contrast, the temporal or spatial frequency defined with respect to time or arc length coordinate scale inversely with duration or overall size of the movement.

Pure Frequency Curves

Ellipses and spirals are examples of curves that can be characterized by single angular frequencies. More generally, we define such "pure frequency" curves by having sinusoidal log curvature profiles:

$$h(\theta) = \epsilon \sin(\nu\theta), \qquad [5]$$

where ν is the frequency and ϵ is the amplitude. ($\epsilon = 0$ describes a circular path shape.) A phase shift could also be added, which rotates the shape.

Some examples of pure frequency curves are shown in Fig. 4. At integer frequencies with $\nu > 2$, these curves resemble rounded regular polygons. In general, a curve with a rational frequency $\nu = m/n$, where m and n are coprime integers (i.e., no common factors) and $m \neq 1$, has a closed shape of period $\Theta = 2\pi n$, and exhibits m degrees of rotational symmetry. If $m = 1$, then the curve exhibits a translational symmetry. A logarithmic spiral is the zero frequency limit of a pure frequency curve: $h(\theta) = \lim_{\nu \to 0}(a/\nu)\sin(\nu\theta) = a\theta$.

Theoretical Prediction. The optimal log speed profile for pure frequency curves can be expanded as a sum of harmonic terms. To first order in ε, the expansion of Eq. **3** yields the following:

$$z(\theta) \approx -\epsilon\beta \sin(\nu\theta), \qquad [6]$$

where the gain is given by the following:

$$\beta(\nu) = \frac{2}{3}\left(\frac{1 + \nu^2/2}{1 + \nu^2 + \nu^4/15}\right), \qquad [7]$$

which provides an excellent approximation over a wide range of amplitude and frequency (*Appendix D*). This first-order approximation describes a linear relationship between log curvature and

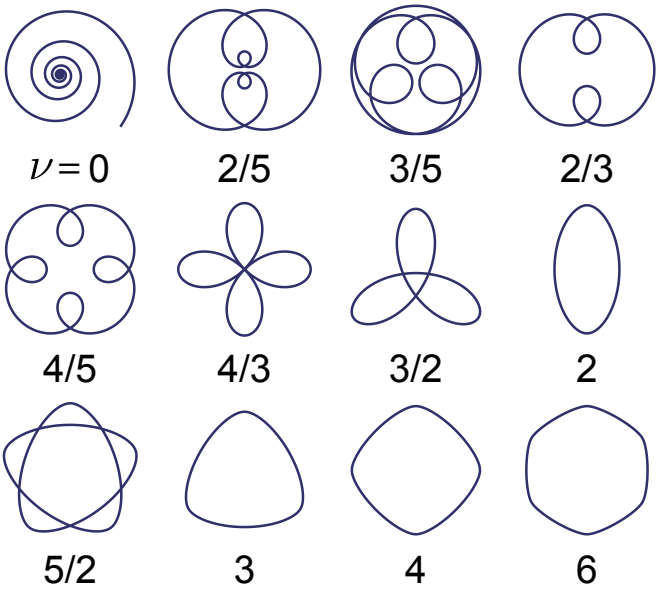

Fig. 4. Examples of pure frequency curves shown with their characteristic frequencies, ν. See https://www.youtube.com/watch?v=waXWOv0YqFE for a movie showing how the shape of the curve varies with continuously changing angular frequency.

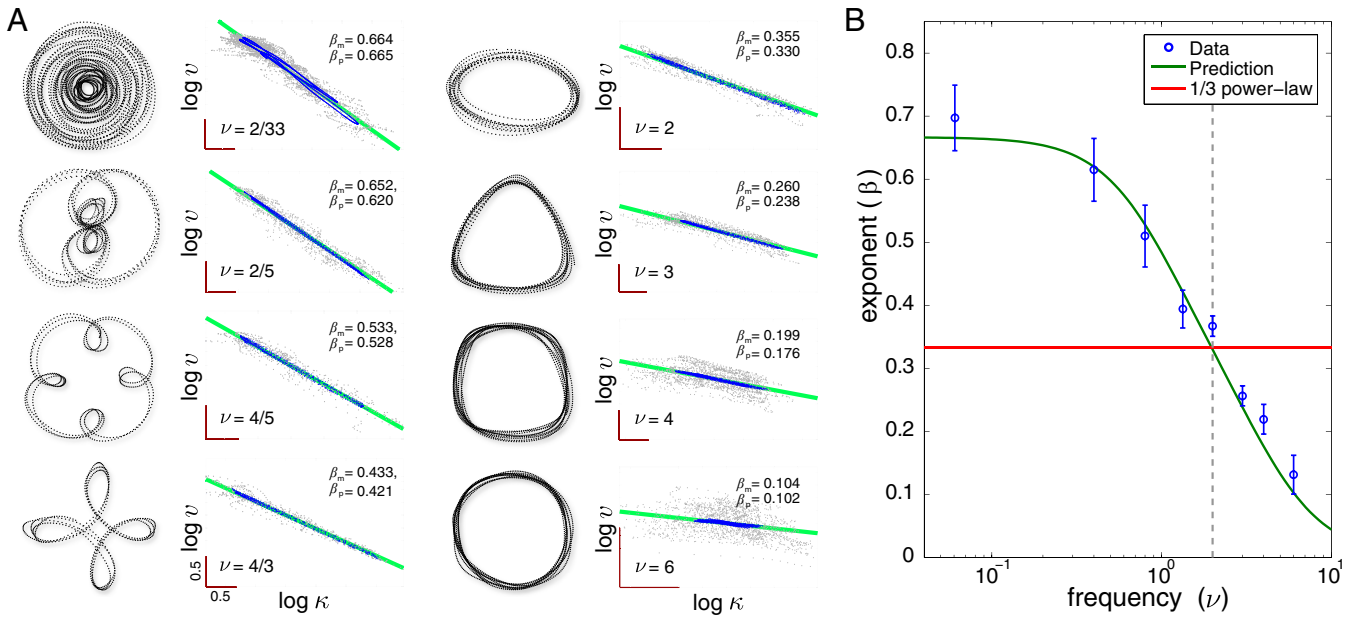

Fig. 5. Measurements of humans drawing pure frequency curves compared with parameter-free model predictions. (*A*) Typical movement examples from a single subject shown to the *Left*. Black dots: movement trajectory data. Log speed vs. log curvature shown to the *Right*. Gray dots: raw curvature–speed data. Blue dots: bandpass-filtered curvature–speed data. Green line: minimum-jerk model prediction. Predicted β_p and measured β_m are given in the *Inset* for each ν. (Scale bar: 0.5.) (*B*) Power law exponents (β) as a function of angular frequency (ν). Blue circles: mean exponent values from $N = 8$ subjects measured from the slopes of $\log v - \log \kappa$ plots. Error bars: SD. Red line: 1/3 power law. Green line: minimum-jerk model prediction.

log speed profiles, or equivalently, a power law relationship between speed and curvature:

$$v(\theta) \propto \kappa(\theta)^{-\beta}. \quad [8]$$

This result predicts a spectrum of power laws for pure frequency movements. The exponent $\beta(\nu)$ is a monotonically decreasing function of the angular frequency, starting from $\beta(0) = 2/3$ for spiral movements, and approaching $\beta \to 0$ as the frequency increases, $\nu \to \infty$. Note that the prediction for ellipses is $\beta(2) = 30/91 \approx 1/3$. In comparison, the one-third power law assumes a constant exponent $\beta = 1/3$ for all shapes.

Experimental Confirmation. We recorded subjects' drawing movements of pure frequency curves to test the prediction of the minimum-jerk model (Fig. 5 and *Materials and Methods*). Because there was motor variability in the movement trajectories around the desired periodic shapes, a bandpass filter was applied to the speed and curvature profiles (*Materials and Methods*).

The log speed vs. log curvature data were scattered around straight lines (gray dots) that became sharper after filtering (blue dots), confirming power law relationships between speed and curvature Fig. 5*A*. Moreover, the slopes of the lines depended on the frequency of the curve in a decreasing manner, which agreed with the model prediction (Fig. 5*B*). Note that the model prediction does not have any free parameters to fit.

Curves with Multiple Shape Features

Elliptic Spiral. Some curves, such as in Fig. 1*B*, cannot be characterized by a single frequency but instead exhibit multiple shape features. A good example is an elliptic-spiral trajectory, that is, an elliptic shape with slowly changing size, which exhibits features of both an ellipse and a spiral; these multifeature movements raise a challenge to the results in the previous section: Given that an elliptic movement and a spiral movement individually follow the 1/3 and the 2/3 power laws, what should the relationship between curvature and speed be for an elliptic-spiral movement?

Experimental data revealed a surprising result: The curvature–speed relationship for elliptic-spiral movements showed characteristics of two power laws (Fig. 6). When plotted on a log–log scale, the data points did not form a line, but a parallelogram, consisting of stacked parallel lines with $-1/3$ slope, with their centers along a line with $-2/3$ slope.

Combining Shape Features. Before we can analyze multifeature movements, we first need to address the following question: How do multiple shape features combine to produce a complex curve shape?

The operation of reshaping a curve with additional shape features can be understood in terms of modifying the curve's length scale. For example, progressively decreasing the length scale of a curve changes its shape to become "spiral-like," whereas elongating the curve in one direction and compressing in the perpendicular direction changes its shape to be "ellipse-like."

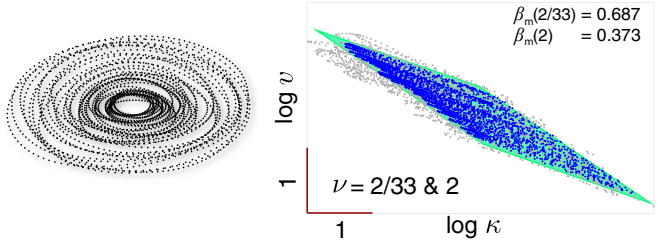

Fig. 6. Elliptic-spiral movement exhibiting a mixture of power laws. (*Left*) Movement trajectory drawn by a subject. (*Right*) Log speed vs. log curvature plot. The filtered data points form a parallelogram with sides having approximately $-1/3$ and $-2/3$ slopes (green region). On each elliptic arc, the points form a straight line with $-1/3$ slope. Successive arcs translate along a broader line with $-2/3$ slope as the ellipse size slowly changes. Gray dots: raw data. Blue dots: smoothed data with a dual-band filter centered at $\nu = 2/33$ and $\nu = 2$. β_m: measured exponent for each frequency band. (Scale bar: 1.0.)

Because the operation of combining multiple shape features is a type of scaling operation, it is most naturally implemented in the scale-invariant, angle coordinate representation—as pointwise addition of the log curvature profiles:

$$h(\theta) = h_1(\theta) + h_2(\theta). \quad [9]$$

This operation indeed correctly combines a spiral and an ellipse to produce an elliptic spiral.

The addition operation, together with scalar multiplication, defines a vector space over the set of convex paths, which is spanned by the basis set of pure frequency curves; that is, any curve in this space can be represented as a linear combination of pure frequency components via the Fourier transform (Fig. 7). See ref. 14 for an in-depth discussion of the vector space of curve shapes.

Mixtures of Power Laws. As already shown for the case of elliptic spirals, multifrequency movements do not exhibit a simple power law relationship between curvature and speed. Instead, the first-order analysis of Eq. **3** predicts mixtures of power law relationships, which is best expressed in the frequency domain as follows:

$$\tilde{z}(\nu) = -\beta(\nu)\tilde{h}(\nu), \quad [10]$$

where $\{\tilde{z}(\nu)\} \equiv \mathcal{F}[\{z(\theta)\}]$, $\{\tilde{h}(\nu)\} \equiv \mathcal{F}[\{h(\theta)\}]$ are, respectively, the Fourier transforms of the log speed and log curvature profiles, and $\beta(\nu)$ is the frequency-dependent exponent shown in Eq. **7**. Therefore, the power law relationship (Eq. **8**) applies to each frequency component of the speed and curvature profiles.

Experimental Confirmation. Subjects were shown path shapes with multiple frequency components and asked to draw the shapes (Fig. 7). Spectral analysis of the movement data indeed showed peaks at the chosen frequencies, for example at 2 and 2/33 for elliptic-spiral movements, and the log speed spectrum predicted by Eq. **10** was confirmed.

We also recorded free-form doodling movements, where the subjects drew random, arbitrary curved shapes. Spectral analysis of these movements revealed multiple peaks as well as broadband power across the spectrum, which also confirmed the predicted log speed spectrum.

Overall, the mixture of power laws explains a greater proportion of the variance in speed profiles than the one-third power law (Fig. 7*G*). This result also confirms that the first-order analysis of the Euler–Lagrange equation (Eq. **3**) is valid for a broad range of hand drawings.

Low-Pass Filter Interpretation

The mixture of power laws (Eq. **10**) describes the relationship between log curvature and log speed profiles as a linear time-invariant operation, where the power law exponent, $\beta(\nu)$, can be interpreted as a gain for the frequency response of a second-order low-pass filter that suppresses high-frequency components of movements. In the angle domain, this relationship is a convolution:

$$z(\theta) = -\left[\tilde{\beta} * h\right](\theta), \quad [11]$$

where $\tilde{\beta}(\theta)$ is the impulse response function of the filter:

$$\tilde{\beta}(\theta) \equiv \mathcal{F}^{-1}[\beta(\nu)] = \frac{5/2}{\gamma_1^2 - \gamma_2^2}\left(\frac{\gamma_1^2 - 2}{\gamma_1}e^{-\gamma_1|\theta|} - \frac{\gamma_2^2 - 2}{\gamma_2}e^{-\gamma_2|\theta|}\right), \quad [12]$$

with decay rates $\gamma_{1,2} = \sqrt{(15 \pm \sqrt{165})/2}$, ($\gamma_1 \cong 3.73$ and $\gamma_2 \cong 1.04$) (Fig. 8).

The symmetric shape of the impulse response function (Eq. **12**) implies that it requires information about the future and the past path shape to plan a curved movement. Moreover, the extent of planning is ≈ 1 radian, which is the approximate width of the impulse response function. In contrast, the one-third power law has a flat frequency response (Fig. 8*A*), and thus a delta function impulse response in the angle domain (Fig. 8*B*), which predicts that the movement speed should be instantaneously determined by the local curvature without any planning.

Discussion

We investigated the minimum-jerk model and derived an analytic expression for the curvature–speed relationship that accounts for a wide range of curved hand movements. Previous studies analyzed the model only for a few selected trajectory shapes and found behavior similar to the one-third power law (3, 8–10). In contrast, our analysis showed that the one-third power law relationship cannot hold universally and instead predicted a continuous spectrum of power laws for pure frequency movements and mixtures of the power laws for general multifrequency movements, which we subsequently confirmed experimentally.

The ansatz was to represent curved paths in terms of their log curvature profiles in a dimensionless angle coordinate. This representation yielded a vector space of curves, in which simple pure frequency curves can be combined to create arbitrarily complex curved paths. Moreover, the pure frequency curves form the eigenbasis of the space for the first-order analysis of the Euler–Lagrange equation that describes the optimal curvature–speed relationship. The power law exponent is the eigenvalue of the relationship, which is a function of the angular frequency—a scale-invariant geometric feature that defines pure frequency curves.

So why has the one-third power law been the dominant regularity reported in the literature? It may be due to too narrow a focus in the space of curved shapes. Indeed, only a few curved shapes have been used in previous studies of hand drawing: Ellipses ($\nu = 2$) have been the most popular shape (5–7, 15); three-lobe ($\nu = 3/2$) or four-lobe ($\nu = 4/3$) cloverleaf shapes have power laws that are close to that of ellipses although they look quite different on the surface (4). A previous perturbation analysis of the minimum-jerk model on these shapes also found exponents close to the one-third power law (10).

Others have studied movements with highly elongated features, such as elliptic-spiral shapes or cursive handwriting, e.g., consecutive l's (1–3), which contain concentrated power near the frequency of ellipses ($\nu \approx 2$) as well as in the low frequency range. These movements generated apparent fragmentation of the one-third power law on the log speed vs. log curvature plots, as though the coefficient of the power law had changed across the movement fragments. Our frequency-based analysis accounts for the fragmentation and the one-third power law as different manifestations of the same general regularity: a spectrum of power laws.

The frequency-dependent power law of curved movements provides a sensitive way to test the validity of various theoretical models for movement control and planning. For example, the equi–affine-speed hypothesis, which assumes the affine-speed of human movement should be held constant, can only generate movements that follow the one-third power law for all planar movements (4, 7), which is inconsistent with our experimental results. However, a recent generalization of the model, which defines speed in a combination of Euclidean, affine, and equi-affine geometries, can generate variable power law exponents (13). The equilibrium point hypothesis paired with low-pass–filtering properties of muscles exhibits one-third power law behavior for ellipse drawing movements, if the equilibrium point moves along the elliptic trajectory with constant speed (5, 6). However, the low-pass filter in such models is defined in the time domain, rather than in the dimensionless angle domain, and is therefore unlikely to generate different power law exponents for different angular-frequency shapes.

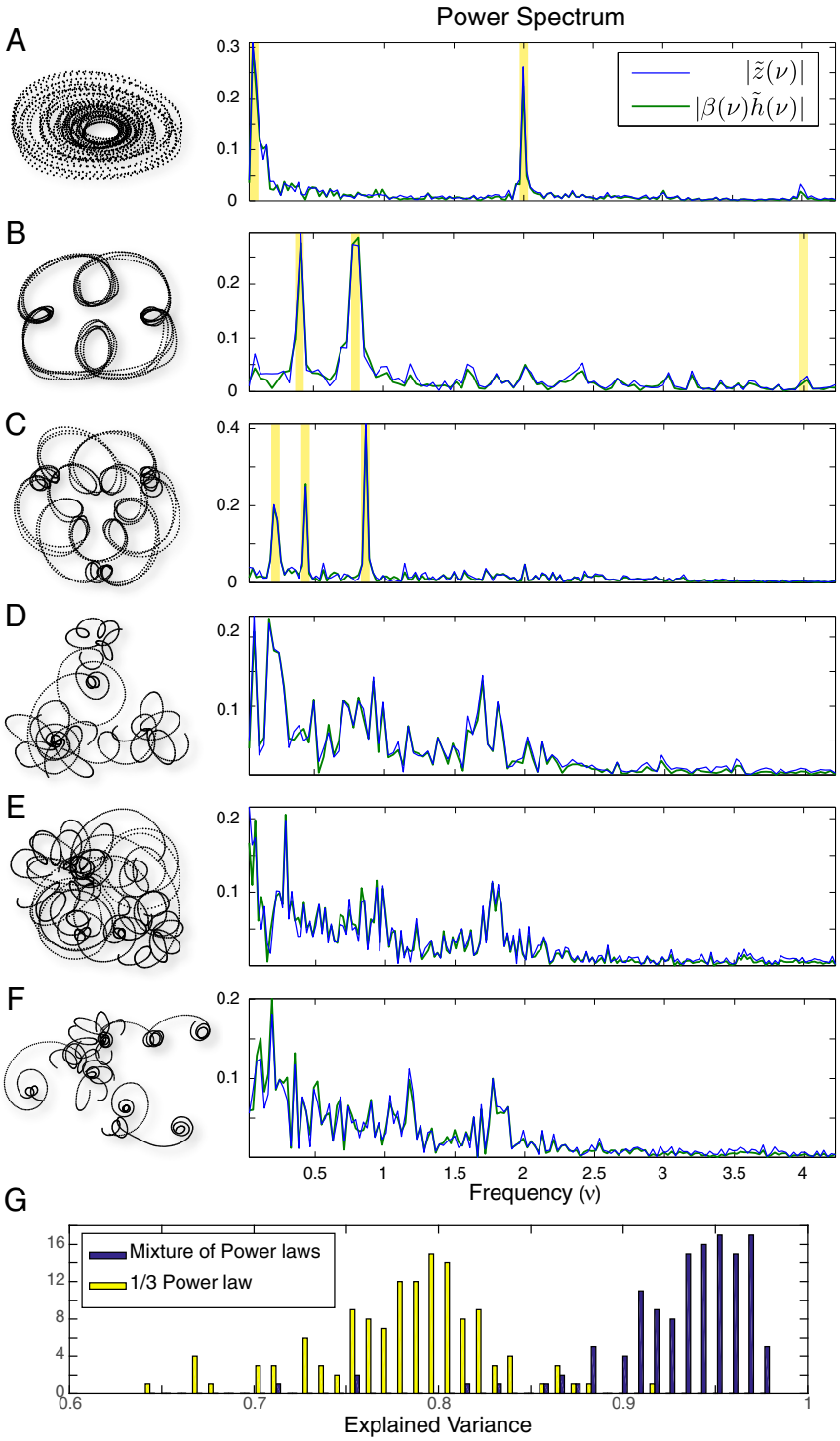

Fig. 7. Complex free-hand movements (*Left*) and corresponding amplitude spectra (*Right*) comparing log speed [$\tilde{z}(\nu)$, blue line] and the power law exponent times log curvature [$\beta(\nu)\tilde{h}(\nu)$, green line]. Vertical yellow bars indicate the specified frequency components. (*A*) An elliptic-spiral movement exhibiting peaks at 2 and 2/33, corresponding to contributions from the elliptical and the spiral components, respectively. (*B*) Multifrequency movements with peaks at 2/5, 4/5, and a minor peak at 4. (*C*) Multifrequency movements with three peaks at 3/14, 3/7, 6/7. (*D*–*F*) Random doodles with broadband power spectra. (*G*) Histogram showing the proportion of the log speed variance explained by the model [$\beta(\nu)\tilde{h}(\nu)$, purple bars] or the 1/3 power law (yellow bars) for multifeature movements, including *A*–*F*.

We showed that the curvature–speed relationship is approximately a linear time-invariant operation that suppresses high angular-frequency components of the speed profile. This leads to an intuition for motor control as a low-pass–filtering operation, which agrees with the observation that human movements tend to maximize smoothness (11). Interestingly, most subjects reported pure frequency movements with high frequencies ($\nu > 3$) to be quite difficult to produce (Fig. 5*A*, frequencies $\nu = 4,6$).

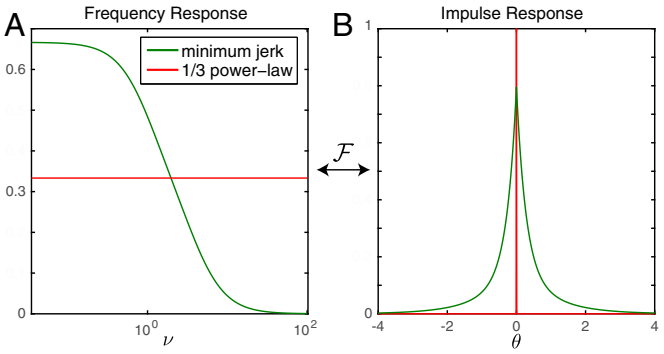

Fig. 8. (*A*) The frequency-dependent power law exponent, $\beta(\nu)$, can be understood as the frequency response function of a linear low-pass filter. The one-third power law has a flat frequency response. (*B*) Corresponding impulse response functions, $\tilde{\beta}(\theta)$. The width of this noncausal filter is ≈ 1 radian. The one-third power law has a delta function impulse response.

Moreover, the amplitude spectra of the log curvature profiles for free-hand doodles often show broad peaks at $\nu = 1.5 \sim 2.5$, which is near the frequency for ellipses, and in low frequencies ($\nu < 1$), but minimal power at high frequencies ($\nu > 3$) (Fig. 7 *D–F*). This may imply that the motor control process also suppresses high-frequency components of the path shape, although the process of selecting movement paths is as yet an unsolved problem.

Remarkably, the low-pass–filtering operation implies that the minimal extent necessary for motor planning has a fixed width of ≈ 1 radian in the angle coordinate. This width, if represented in time or distance, would scale with the speed or size of movements: Slower or larger movements would require planning over a longer time or distance. This insight also applies to planning for a straight reaching movement, which requires complete information of the trajectory from the start to the goal. However, if the planning duration exceeds the capacity of working memory, which might happen for very slow movements, the regularities observed for normal movements may break down.

In this study, we used an angle coordinate for representing movements, which was central in analyzing scale-invariant properties of movements, such as the exponent of the power law relationship. The same dimensionless representation may also be useful in analyzing other scale-invariant features and reveal spectrum of power laws in other motor contexts. Power laws have indeed been observed in many types of movements, including 3D hand movements (16), smooth pursuit eye movements (17), speech (18), and walking (19), and also appear in visual motion perception (20).

The angle coordinate representation may be relevant for interpreting neurophysiological data as well: Power laws have been reported in neural activity recorded in premotor and motor cortices (21, 22), and many neurons in the motor cortex show preference for the direction of movement (23). This is consistent with motor planning based on a form of the angle coordinate representation for generating motor kinematics and dynamics in an allocentric reference frame (24). Scale invariance may be a general principle used by the motor system for organizing complex movements, and analyzing neurophysiological data in the angle coordinate representation may reveal new aspects of neural control of movements.

Materials and Methods

Experimental Method. A commercial tablet device (Wacom Cintiq 24HD graphic monitor) was used to record movement trajectories. The sampling rate of the digitizer was 200 Hz, and the accuracy of the recorded position was 0.05 mm. The passive sensor of the digitizer was attached to the forefinger tip to allow free movement of the hand. Hand movements were recorded from 10 20- to 30-y-old subjects without known motor disorders. The subjects traced shapes that were displayed on the screen of the tablet monitor (pure and multifrequency curves), as well as free-hand doodles, and were encouraged to draw the shapes fluidly without making corrections. University College London institutional ethics and Salk institutional review board approval were obtained for the study, and participants provided written informed consent.

Analysis. The movement velocity profile was obtained by smoothly differentiating the trajectory (25). The speed profile and the curvature profile were then derived as $v(t) = ||\vec{v}||_2$, $\kappa(t) = v^{-1} d\theta/dt$, where $\theta(t)$ was the continuous angle profile of movement velocity: $\theta(t) = \text{unwrap}(\text{angle}(\vec{v}))$. Frequency analysis of the log speed and the log curvature profiles were obtained by first spline-fitting the profiles, resampling with uniform step size in angle coordinate, and applying the Fourier transform. For the analysis in Fig. 5, the data were filtered with a bandpass filter around the target frequency ν_o: $e^{-5\nu_o \log_2(\nu/\nu_o)^2}$.

Appendix A: Jerk Cost in the Angle Coordinate Representation

In the 2D Euclidean frame and time coordinate representation, the velocity vector is expressed as $\vec{v} = v_x\hat{x} + v_y\hat{y}$, and the squared-jerk cost is as follows:

$$\mathcal{L} = \left|\left|\frac{d^2\vec{v}}{dt^2}\right|\right|^2 = \left(\frac{d^2v_x}{dt^2}\right)^2 + \left(\frac{d^2v_y}{dt^2}\right)^2,$$

and the total cost is $\int_0^T \mathcal{L}dt$. Instead, we use the Frenet–Serrett frame and angle coordinate representation, whose orthonormal basis vectors are the tangent and the normal vectors, $\hat{t}, \hat{n}$, which rotate with the angle coordinate as follows:

$$\dot{\hat{t}} = \hat{n}, \qquad \dot{\hat{n}} = -\hat{t},$$

where the dot notation represents differentiation by angle. In this representation, the velocity vector and its time derivatives are expressed as follows:

$$\vec{v} = v\hat{t},$$

$$\frac{d\vec{v}}{dt} = \kappa v^2(z\hat{t} + \hat{n}),$$

$$\frac{d^2\vec{v}}{dt^2} = \kappa^2 v^3\left(\left(2z^2 + \dot{z} + hz - 1\right)\hat{t} + \left(3z + h\right)\hat{n}\right),$$

where time differentiation is converted to angle differentiation via the conversion factor, $d\theta/dt = \kappa v$, and $z = \log(v/v_o)$, $h = \log(\kappa/\kappa_o)$ are, respectively, the log speed and the log curvature (with

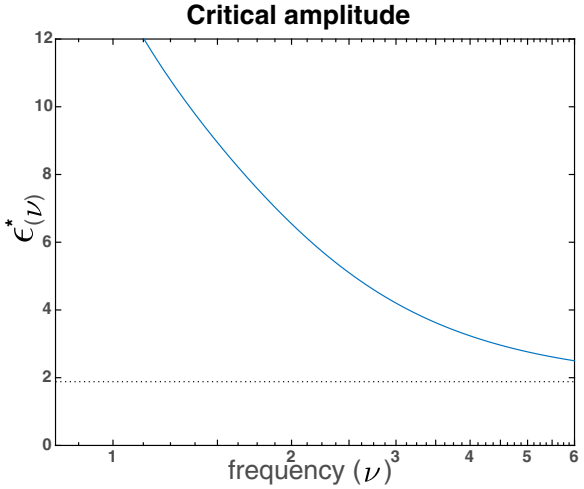

Fig. 9. Critical amplitude, $\epsilon^*(\nu) = |a_1(\nu)/a_2(\nu)|$. The asymptote at high frequencies is $\epsilon^*(\infty) = 32/17$ (dotted line).

arbitrary normalization constants v_o, κ_o). Therefore, the instantaneous cost for the minimum-jerk problem becomes the following:

$$\tilde{\mathcal{L}} = \frac{\kappa^4 v^6 \left(\left(2\dot{z}^2 + \ddot{z} + \dot{h}\dot{z} - 1 \right)^2 + \left(3\dot{z} + \dot{h} \right)^2 \right) + \lambda}{\kappa v},$$

such that the total cost is $\int_{\theta_i}^{\theta_f} \tilde{\mathcal{L}}\, d\theta = \int_{t_i}^{t_f} (\mathcal{L} + \lambda) dt$, where λ is the Lagrange multiplier for the duration constraint.

Appendix B: Euler–Lagrange Equation in Angle Coordinate

The optimality condition for the speed profile is given by the Euler–Lagrange equation:

$$\frac{\partial \tilde{\mathcal{L}}}{\partial z} - \frac{d}{d\theta}\left(\frac{\partial \tilde{\mathcal{L}}}{\partial \dot{z}} \right) + \frac{d^2}{d\theta^2}\left(\frac{\partial \tilde{\mathcal{L}}}{\partial \ddot{z}} \right) = 0.$$

Partial derivatives of the cost function are as follows:

$$\frac{\partial \tilde{\mathcal{L}}}{\partial z} = 5\kappa^3 v^5 \left(\left(\ddot{z} + \dot{h}\dot{z} + 2\dot{z}^2 - 1 \right)^2 + \left(\dot{h} + 3\dot{z} \right)^2 \right) - \frac{\lambda}{\kappa v},$$

$$\frac{\partial \tilde{\mathcal{L}}}{\partial \dot{z}} = 2\kappa^3 v^5 \left(\left(\dot{h} + 4\dot{z} \right)\left(\ddot{z} + \dot{h}\dot{z} + 2\dot{z}^2 - 1 \right) + 3\left(\dot{h} + 3\dot{z} \right) \right),$$

$$\frac{\partial \tilde{\mathcal{L}}}{\partial \ddot{z}} = 2\kappa^3 v^5 \left(\ddot{z} + \dot{h}\dot{z} + 2\dot{z}^2 - 1 \right),$$

where $\partial v / \partial z = v$ is used, because $v = v_o e^z$. Proceeding with differentiation by θ and collecting the terms yield the following:

$$\begin{aligned} \lambda = \kappa^4 v^6 \Big(& 5 + 2\dddot{z}\dot{z} - 30\ddot{z} - 10\ddot{h} - 25\dot{h}^2 + 82\dot{h}\dot{z}^3 + 40\dot{z}^4 \\ & + \dot{z}\left(2\dddot{h} + 14\ddot{h}\dot{h} - 90\dot{h} + 12\dot{h}^3 \right) \\ & + \dot{z}^2\left(20\ddot{h} + 55\dot{h}^2 - 75 \right) + 15\ddot{z}^2 \\ & + \ddot{z}\left(82\dot{z}^2 + 90\dot{h}\dot{z} + 8\ddot{h} + 22\dot{h}^2 \right) + \dddot{z}\left(20\dot{z} + 12\dot{h} \right) \Big). \end{aligned} \quad [13]$$

Appendix C: Logarithmic Spiral

The optimality condition (Eq. **13**) can be exactly solved for a logarithmic spiral: $h(\theta) = a\theta$. By assuming a linear form for the log speed profile, $z(\theta) = b\theta$, Eq. **13** reduces to the following:

$$\frac{\lambda}{k_o^4 v_o^6} e^{-(4a+6b)\theta} = 5 - a^2\left(25 + 90\frac{b}{a} + 75\frac{b^2}{a^2} \right) + a^4\left(12\frac{b}{a} + 55\frac{b^2}{a^2} + 82\frac{b^3}{a^3} + 40\frac{b^4}{a^4} \right).$$

Because the right-hand side is constant, $4a + 6b = 0$, which yields the 2/3 power law relationship:

$$v(\theta) = v_o \left(\frac{\kappa(\theta)}{\kappa_o} \right)^{-2/3}, \quad [14]$$

where v_o satisfies $\lambda / (k_o^4 v_o^6) = 5 + 5a^2/3 + 4a^4/81$.

Appendix D: Perturbation Expansion

For a pure frequency log curvature profile, $h(\theta) = \epsilon e^{i\nu\theta}$, the optimal log speed profile can be expanded in power series of ε as follows:

$$z(\theta) = a_1 \epsilon e^{i\nu\theta} + a_2 \left(\epsilon e^{i\nu\theta} \right)^2 + \cdots$$

with the coefficients obtained from Eq. **13**:

$$a_n = \frac{(-4)^n}{6 \cdot n!} I_n(\nu). \quad [15]$$

For example, the first three terms in this series expansion are as follows:

$$a_1 = -\frac{2}{3} I_1(\nu), \quad a_2 = \frac{4}{3} I_2(\nu), \quad a_3 = -\frac{16}{9} I_3(\nu), \ldots$$

where

$$I_1 = \frac{1 + \nu^2/2}{1 + \nu^2 + \nu^4/15},$$

$$I_2 = \frac{\left(1 - \frac{5}{8}\nu^2 \right) - 2I_1\left(1 - \frac{3}{4}\nu^2 - \frac{11}{60}\nu^4 \right) + I_1^2\left(1 - \frac{5}{6}\nu^2 - \frac{7}{18}\nu^4 \right)}{1 + 4\nu^2 + \frac{16}{15}\nu^4}.$$

Note that the critical amplitude at which the second-order term becomes comparable to the first-order term is as follows:

$$\epsilon^* = \left| \frac{a_1}{a_2} \right| = \left| \frac{I_1(\nu)}{2I_2(\nu)} \right|, \quad [16]$$

which is a decreasing function of ν with a minimum $\lim_{\nu \to \infty} \epsilon^* = 32/17$ (Fig. 9). Below this amplitude, the first-order approximation provides a good description of the solution.

ACKNOWLEDGMENTS. This research was supported by the Temporal Dynamics of Learning Center (NSF SBE 0542013), the Gatsby Charitable Foundation, and Howard Hughes Medical Institute.

1. Lacquaniti F, Terzuolo C, Viviani P (1983) The law relating the kinematic and figural aspects of drawing movements. *Acta Psychol (Amst)* 54(1-3):115–130.
2. Viviani P, Cenzato M (1985) Segmentation and coupling in complex movements. *J Exp Psychol Hum Percept Perform* 11(6):828–845.
3. Viviani P, Flash T (1995) Minimum-jerk, two-thirds power law, and isochrony: Converging approaches to movement planning. *J Exp Psychol Hum Percept Perform* 21(1):32–53.
4. Flash T, Handzel AA (2007) Affine differential geometry analysis of human arm movements. *Biol Cybern* 96(6):577–601.
5. Gribble PL, Ostry DJ (1996) Origins of the power law relation between movement velocity and curvature: modeling the effects of muscle mechanics and limb dynamics. *J Neurophysiol* 76(5):2853–2860.
6. Schaal S, Sternad D (2001) Origins and violations of the 2/3 power law in rhythmic three-dimensional arm movements. *Exp Brain Res* 136(1):60–72.
7. Pollick FE, Sapiro G (1997) Constant affine velocity predicts the 1/3 power law of planar motion perception and generation. *Vision Res* 37(3):347–353.
8. Wann J, Nimmo-Smith I, Wing AM (1988) Relation between velocity and curvature in movement: Equivalence and divergence between a power law and a minimum-jerk model. *J Exp Psychol Hum Percept Perform* 14(4):622–637.
9. Todorov E, Jordan MI (1998) Smoothness maximization along a predefined path accurately predicts the speed profiles of complex arm movements. *J Neurophysiol* 80(2):696–714.
10. Richardson MJE, Flash T (2002) Comparing smooth arm movements with the two-thirds power law and the related segmented-control hypothesis. *J Neurosci* 22(18): 8201–8211.
11. Flash T, Hogan N (1985) The coordination of arm movements: an experimentally confirmed mathematical model. *J Neurosci* 5(7):1688–1703.
12. Kant K, Zucker SW (1986) Toward efficient trajectory planning: The path-velocity decomposition. *Int J Robot Res* 5(3):72–89.

13. Bennequin D, Fuchs R, Berthoz A, Flash T (2009) Movement timing and invariance arise from several geometries. *PLoS Comput Biol* 5(7):e1000426.
14. Huh D (2015) The vector space of convex curves: How to mix shapes. arXiv: 1506.07515.
15. Viviani P, Schneider R (1991) A developmental study of the relationship between geometry and kinematics in drawing movements. *J Exp Psychol Hum Percept Perform* 17(1):198–218.
16. Maoz U, Berthoz A, Flash T (2009) Complex unconstrained three-dimensional hand movement and constant equi-affine speed. *J Neurophysiol* 101(2):1002–1015.
17. de'Sperati C, Viviani P (1997) The relationship between curvature and velocity in two-dimensional smooth pursuit eye movements. *J Neurosci* 17(10):3932–3945.
18. Tasko SM, Westbury JR (2004) Speed–curvature relations for speech-related articulatory movement. *J Phonetics* 32(1):65–80.
19. Ivanenko YP, Grasso R, Macellari V, Lacquaniti F (2002) Control of foot trajectory in human locomotion: Role of ground contact forces in simulated reduced gravity. *J Neurophysiol* 87(6):3070–3089.
20. Viviani P, Stucchi N (1992) Biological movements look uniform: Evidence of motor-perceptual interactions. *J Exp Psychol Hum Percept Perform* 18(3): 603–623.
21. Schwartz AB (1994) Direct cortical representation of drawing. *Science* 265(5171): 540–542.
22. Schwartz AB, Moran DW (2000) Arm trajectory and representation of movement processing in motor cortical activity. *Eur J Neurosci* 12(6):1851–1856.
23. Georgopoulos AP, Kalaska JF, Caminiti R, Massey JT (1982) On the relations between the direction of two-dimensional arm movements and cell discharge in primate motor cortex. *J Neurosci* 2(11):1527–1537.
24. Tanaka H, Sejnowski TJ (2013) Computing reaching dynamics in motor cortex with Cartesian spatial coordinates. *J Neurophysiol* 109(4):1182–1201.
25. Holoborodko P (2008) Smooth noise robust differentiators. Available at www.holoborodko.com/pavel/numerical-methods/numerical-derivative/smooth-low-noise-differentiators/. Accessed June 23, 2015.